RSC Advances

ROYAL SOCIETY OF CHEMISTRY

www.rsc.org/advances

Novel Co-Ni-Graphene Composite Electrodes for Hydrogen Production

B. Subramanya, Y. Ullal, S. U. Shenoy, D. K. Bhat* and A. C. Hegde

Department of Chemistry

National Institute of Technology Karnataka, Surathkal, Mangalore-575 025, India.

*Corresponding author

E-mail: denthajekb@gmail.com,

Tel: +91-824-2473202; Fax: +91-824-74033/2474082.

Table of Contents (TOC)

A novel, highly efficient composite electrode containining earth-abundant elements (Co-Ni) and graphene has been developed for electrocatalytic hydrogen evolution reaction in alkaline medium.

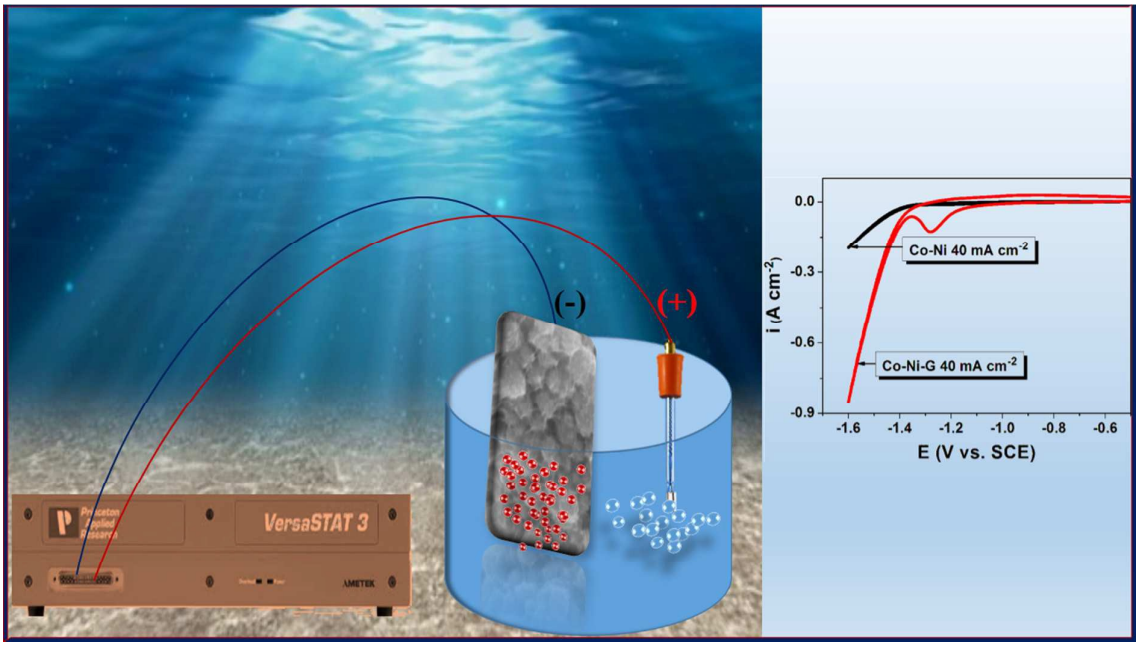

Abstract

Active, stable and cost-effective electrocatalysts are a key to water splitting for hydrogen production through electrolysis. Herein, we report the facile preparation of highly porous Co-Ni-Graphene (Co-Ni-G) composite electrode by electrodeposition for electrocatalytic applications. The incorporation of graphene into Co-Ni matrix enhances the catalyst's activity for hydrogen evolution reaction (HER) in alkaline solution. The best coating exhibits a maximum current density of -850 mA cm^{-2} at -1.6 V, which is approximately 4 times better than that of binary Co-Ni alloy indicating higher activity for hydrogen production. Addition of graphene to electrolyte bath results in porous encapsulated bundle of alloy nano-particles within the graphene network which effectively increases the elelctrochemically active surface area. As indicated by XPS analysis results, on addition of graphene Co(0) and Ni(0) content in the deposit increases and as a result both cobalt/cobalt oxide and nickel/nickel oxide sites are evenly distributed on Co-Ni-G electrode surface which is responsible for increased HER activity. The Tafel slope analysis showed that the HER follows Volmer-Tafel mechanism. The structure-property relationship of Co-Ni-G composite coating has been discussed by interpreting field emission scanning electron microscopy (FESEM), X-ray photoelectron spectroscopy (XPS) and X-ray diffraction (XRD) analysis results.

Keywords: Electrocatalyst, electrodeposition, hydrogen evolution reaction, graphene, composite coating.

Introduction

The global demand for energy is increasing rapidly and continuously during the last few decades. The need for an eco-friendly, renewable and efficient energy source with the potential to replace the commonly used nuclear and fossil fuels is growing each day.[1] Hydrogen, a renewable and clean fuel, is considered as a potential energy carrier for future energy infrastructure.[2, 3] The electrocatalytic splitting of water by HER is an important process with high energy conversion efficiency for hydrogen production.[4] Generally accepted reaction mechanism in alkaline solution is [5]

1) electrochemical hydrogen adsorption (Volmer reaction) [Eq. (1)]

$$H_2O + M + e^- \rightleftharpoons M - H^* + OH^- \quad (1)$$

followed by

2) electrochemical desorption (Heyrovsky reaction) [Eq. (2)]

$$M - H^* + H_2O + e^- \rightleftharpoons M + OH^- + H_2 \uparrow \quad (2)$$

or

3) chemical desorption (Tafel reaction) [Eq. (3)]

$$2\,M - H^* \rightleftharpoons 2M + H_2 \uparrow \quad (3)$$

where H* designates a hydrogen atom chemically adsorbed on an active site of the electrode surface (M).

The use of electrolytic devices to produce hydrogen is generally linked to its energetic properties or commercial interests. In any industrial electrolyzers, the main properties of electrode to be considered for water electrolysis are: large active surface area, electrochemical stability, good electrical conductivity, low hydrogen over-potential, good electrocatalytic activity and high corrosion resistance. Currently, the state-of-the-art catalysts are based on precious metals such as Pt because of their low overpotential and fast kinetics for driving HER.[6, 7] However, the major drawbacks of Pt catalysts are their high cost and limited world-wide supply of these noble metals.[8] To assure sustainable hydrogen production, the cost-effective alternatives to precious Pt featuring high electrocatalytic activities and robust stabilities should be developed. In this context, various earth-abundant transition metals (Fe, Co, Ni, Mo) and their compounds have been designed and developed as highly efficient HER electrocatalysts under either acidic or alkaline conditions.[9-11] However, these materials show inherently high over-potential which needs to be reduced by proper manipulation of their synthetic routes. Several electrodeposited transition metals (like Ni, Co, Fe, Mo and Cu) and their mutual alloys have been used as electrodes for electrolysis of water.[12-19] This is due to the fact that electrodeposition being an atomistic deposition process, the property of the coatings can be controlled closely by regulating the deposition parameters and the bath composition. Moreover, such electrodeposited materials do not require any post-preparation treatment before using them as electrocatalysts.[20] Also, development of nanostructured electrocatalysts with preferentially exposed active sites leads to increased performance. Recently the electrodeposition and electrocatalytic activity of nanostructured Co-Ni alloy coating was reported by our group.[21] Strikingly, some carbon-based materials with unique electronic properties have been also considered as innovative alternatives for Pt catalyst.[22, 23]

Graphene, the 2D form of carbon, has gained great scientific consideration in recent years pertaining to its extraordinary electronic and mechanical properties like high mobility of charge carriers, high thermal conductivity, high mechanical strength, extremely large surface area, etc.[24-26] These noteworthy properties of graphene make it well suited for many applications such as graphene-based electronics, composite materials, molecular gas sensors, energy storage and conversion.[26-30] Graphene, as defined, is a single layer two-dimensional material, comprising of carbon atoms arranged in a hexagonal manner, but graphene samples with two layers (bi-layer graphene) and more than two but less than ten layers (few-layer graphene) are equally of interest.

In view of the aforesaid aspects and as a part of our ongoing research program on synthesis and applications of graphene[31, 32] we thought it is worthwhile to investigate HER experiments employing transition metal alloy-graphene composite electrode. Accordingly, we report herein the fabrication of a novel electrodeposited Co-Ni-G composite electrode and studies on its performance as cathode for HER. The study was aimed at combining the high surface area of graphene with electrocatalytic property of Co-Ni alloys to obtain hybrid porous electrodes from a single step electrodeposition. The porosity of non-precious metal electrocatalysts are generally increased mainly by leaching out certain metals from electrodeposited coatings to impart porosity to the surface.[33, 34] The present single step electrodeposition method eliminates requirement of post treatment of electrodeposited samples and hence they can be directly used for HER. We

have carried out the electrodeposition of nanocrystalline Co-Ni-G composite coating and have studied their applicability to HER or water splitting reaction in alkaline medium. The effect of graphene on electrocatalytic and physical properties of the coatings have been studied systematically and the observed results are discussed in the following sections.

Materials and methods

Electrodeposition of Co-Ni-G composite coating

The electrodeposition of Co-Ni-G electrocatalyst was accomplished in an acid sulphate bath with composition and operating parameters as given in Table 1.

Table 1 Composition and operating parameters for deposition of Co-Ni-G composite coatings on copper substrate.

Composition	Concentration ($g\ L^{-1}$)	Operating Parameter
$NiSO_4.6H_2O$	100	Cathode: Pure Cu
$CoSO_4.7H_2O$	25	Anode: Pure Ni
Boric acid	20	Temperature: 303K
Ascorbic acid	5	pH: 3.5
Sodium lauryl sulfate	1	Current density: 10 – 40 mA cm^{-2}

0.5 g L^{-1} synthesized graphene was added to obtain Co-Ni-G composite coatings.

Co-Ni-G composite coatings were deposited on a cross sectional area of copper rod using a customized glass cell having a total volume capacity of 225 mL. Mirror polished copper surface (exposed area of 1.0 cm^2) was electro-cleaned and then pickled in a mixture of 0.5 M HNO_3 and 0.5 M H_2SO_4 to activate the surface. Pure Ni plate with equal exposed surface area was used as an anode. The cathode and anode were placed parallel at 5 cm distance during plating. 0.5 g L^{-1} of synthesized graphene (ESI†) was added into Co-Ni bath. Then bath was agitated ultrasonically for 48 hours to ensure uniform dispersion of graphene. Agilent N6705A DC power analyser was used as a high sensitive power source for electrodeposition. The total time for electrodeposition was fixed at 900 s in all the cases. To compare the electrocatalytic properties of Co-Ni-G composite coatings with Co-Ni alloy coatings we have carried out the electrodeposition of Co-Ni alloy on copper substrate and characterized as per the reported procedure.[21]

Characterization

The surface morphology of electrodeposited coatings were characterized by FESEM. The elemental composition and phase structures were analysed using XPS and XRD techniques, respectively. Electrocatalytic study of Co-Ni alloy and Co-Ni-G composite coatings were carried out using a custom made three-electrode tubular glass cell, with arrangements as shown in Fig. 1.

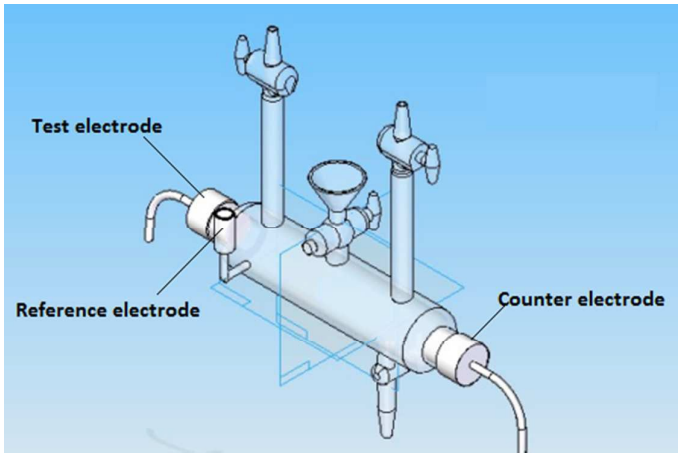

Fig. 1 Customised tubular 3-electrode cell with provision to collect liberated H_2 on the electrode surface.

The electrochemical cell was designed for quantitative measurement of hydrogen, where electrodeposited Co-Ni-G composite electrode was subjected to cathodic and anodic polarization, respectively. Electrodeposited Co-Ni-G composite coatings obtained under different deposition conditions were used as the test electrode and platinum electrode of the same surface area (1.0 cm^2) was used as the counter electrode. Saturated calomel electrode (SCE) was used as the reference electrode. All potentials reported in the present study are with reference to SCE. Luggin's capillary with agar-KCl salt bridge was used to minimize the error due to Ohmic drop.

Electrochemical behaviour of the coatings, in terms of HER, was evaluated by subjecting it to cyclic voltammetry and chrono-potentiometry studies in 6 M KOH medium, using computer controlled potentiostat VersaStat3-400 (Princeton Applied Research, USA). The cell was fitted with a graduated gas collector where the liberated hydrogen replaces corresponding amount of solution. This facility allows relating the amount of gas liberated at given time for electrode materials deposited at a given current density.

Results and discussion

The composition and operating parameters of the bath used for deposition of Co-Ni-G composite coating in the present study is given in Table 1. The plating parameters and bath composition used were optimized by standard Hull cell method described elsewhere.[35] Co-Ni-G composite coatings have been deposited on cross sectional area of copper rod using customised glass cell at different current densities (*i*) i.e., 10, 20, 30 and 40 mA cm^{-2}. The deposits were analysed for surface morphology and compositional variation with applied current density.

Surface and compositional characterization

FESEM analysis

Electrocatalysis is a heterogeneous process and is a function of surface morphology of the electrode material. The accepted mechanism for HER proceeds through an adsorption step basically. Hence, it is the surface structure and morphology that is vital in electrocatalytic materials developed by electrodeposition. The structure and morphology of Co-Ni alloy coating surfaces were reported in the literature by our group in our previous study.[21] It was observed that at all current densities the grain size as observed in FESEM images were in the nanometric range. Also, with the increase in current density, the deposit became coarse and rough, increasing its specific surface area (ESI†).

With the addition of graphene to the deposition bath, as expected a change in surface morphology of the coatings is observed. The FESEM images at different magnifications for Co-Ni-G composite coating deposited from optimal bath at 40 mA cm^{-2} are shown in Fig. 2. Fig. 2a shows irregular 3-dimensional structures scattered all over the surface of the deposit. The synthesized graphene has a high specific surface area of 2276.1 $m^2 g^{-1}$ and hence the adsorption of electrolyte solution onto graphene is expected to be very high. On applying current, the electrolyte adsorbed graphene layers get dragged towards the cathode and gets incorporated into it along with the growing alloy layer. The adsorbed metal ions on the graphene get reduced into metal atoms and deposit as an encapsulated bundle of alloy nano-particles within the graphene network (Fig. 2b and 2c). Such structural changes due to the addition of graphene increase the surface roughness and hence increase the electroactive surface area of the composite coating, which in turn enhances the electrocatalytic activity of binary alloy coating. Hence, this approach of preparing nano-porous electrodes is a very promising method, as it does not require any sophisticated set-up or post treatment of leaching out one of the metal or etching from metal matrices.

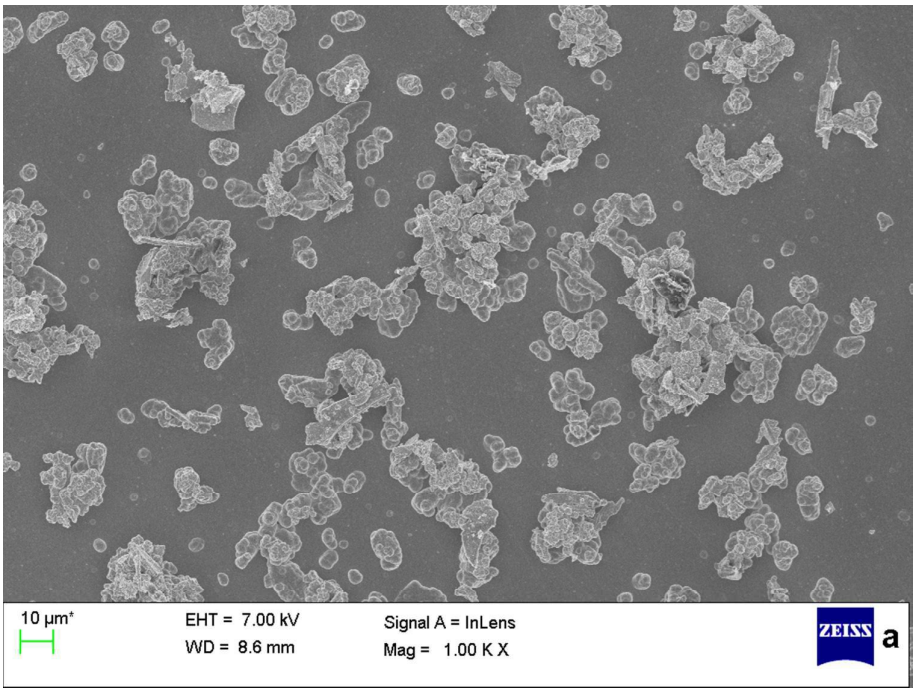

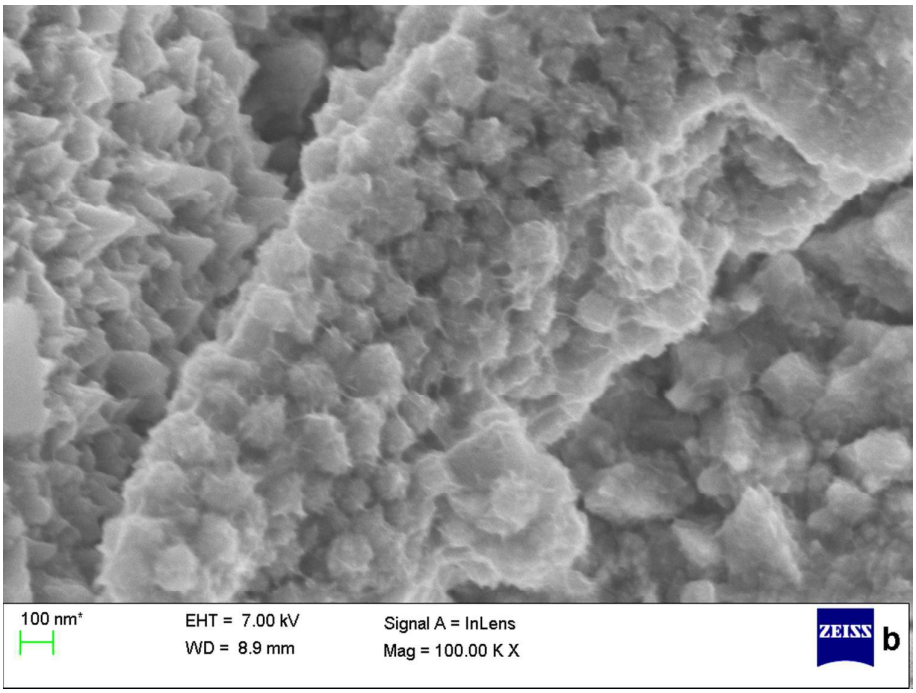

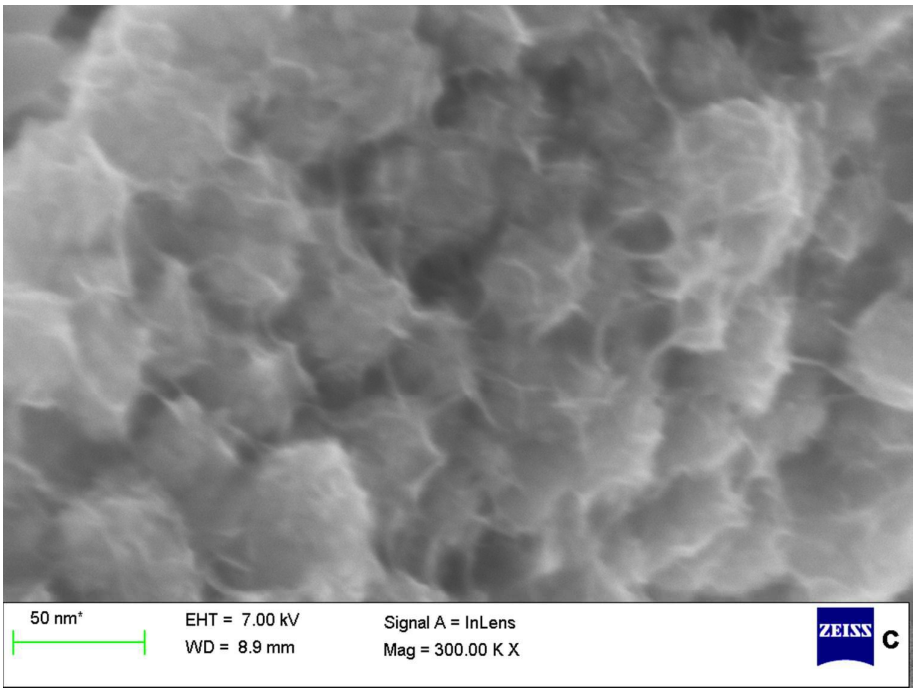

Fig. 2 FESEM images of (a) Co-Ni-G composite coating deposited from optimal bath at 40 mA cm^{-2} displaying irregularly shaped graphene layers embedded in Co-Ni alloy matrix; (b) and (c) magnified images showing encapsulated bundle of alloy nano-particles within the graphene network.

XPS analysis

XPS studies of solid material offer very useful information on elemental composition both on the surface and the bulk of the sample (up to few layers). Similarly, this technique was used to evaluate the surface deposits of Co-Ni alloy and Co-Ni-G composite coatings, which were obtained galvanostatically at 40 mA cm^{-2}. The wide scan spectrum of Co-Ni alloy and Co-Ni-G composite coatings are shown in Fig. 3a and 3b, respectively.

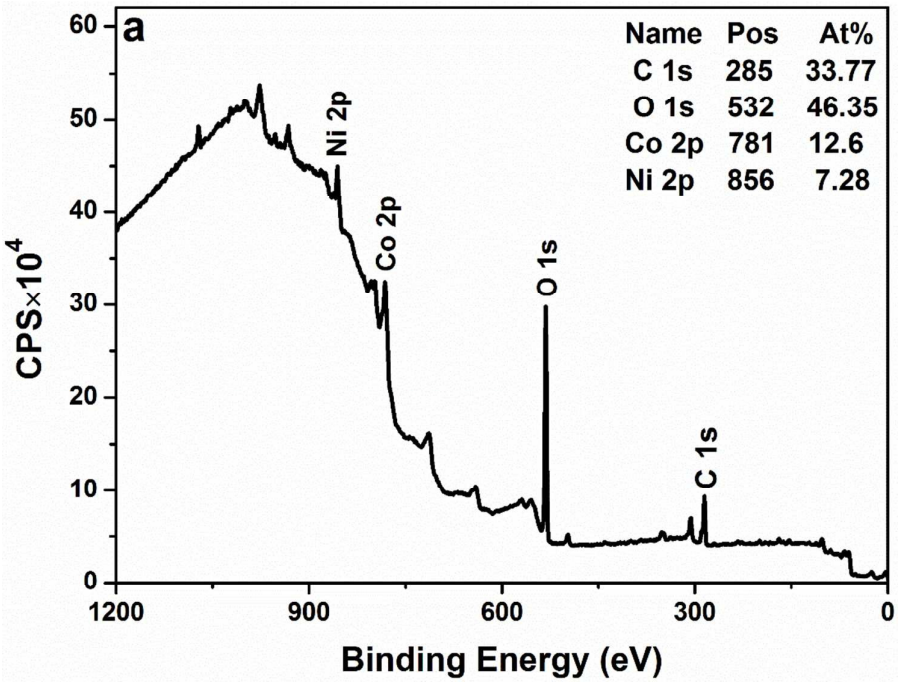

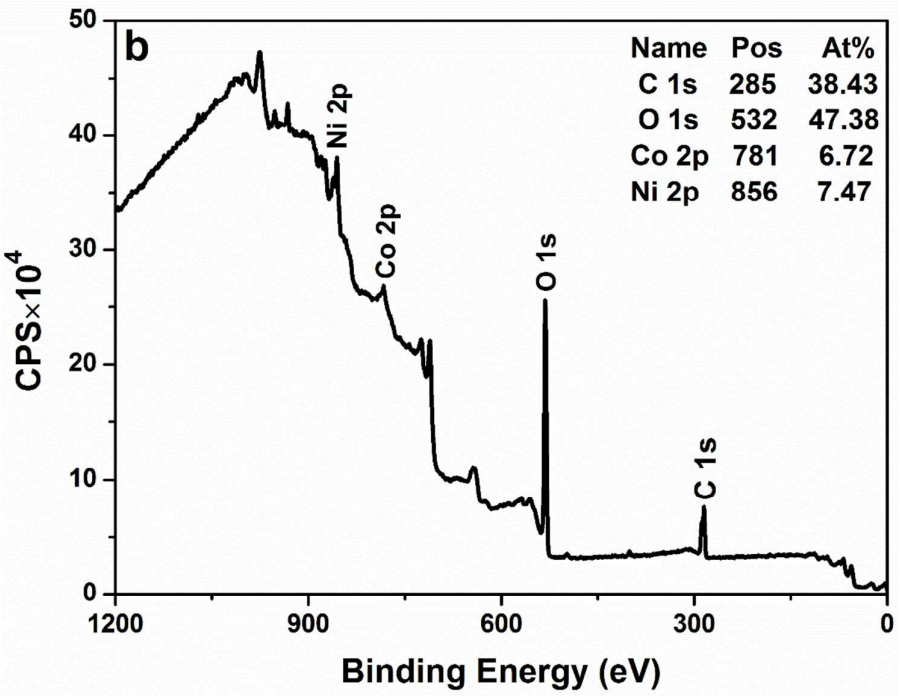

Fig. 3 Wide scan XPS spectrum of (a) Co-Ni and (b) Co-Ni-G.

The deconvoluted C1s spectrum of Co-Ni alloy coating is as shown in Fig. 4a. The fitting analysis shows two strong peaks at 285.5 eV corresponding to sp^3 carbon[36] and 290.5 eV corresponding to occluded CO_2.[37] The sp^3 carbon peak is from ascorbic acid and sodium lauryl sulfate which are added to optimise the bath. The deconvolution of C1s spectrum of Co-Ni-G composite coating reveals a strong and sharp peak at 284.5 eV corresponding to graphitic sp^2 carbon (Fig. 4b).[36, 38] The intensity of sp^3 carbon peak at 285.5 eV is greatly reduced indicating preferential deposition of graphene over amorphous carbon. For similar reasons the intensity of occluded CO_2 peak at 290.5 eV is also reduced.

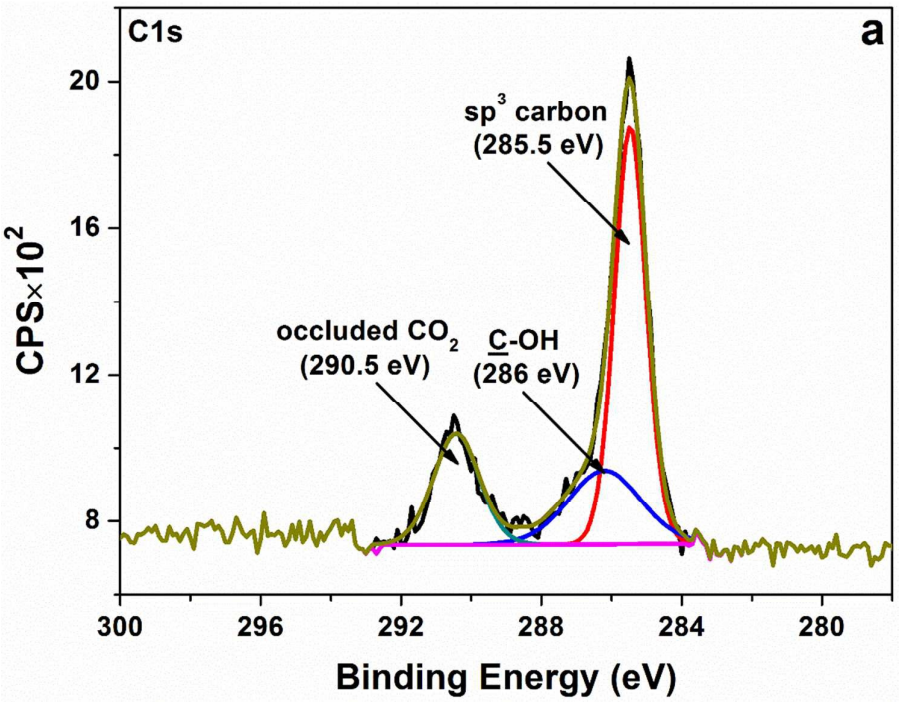

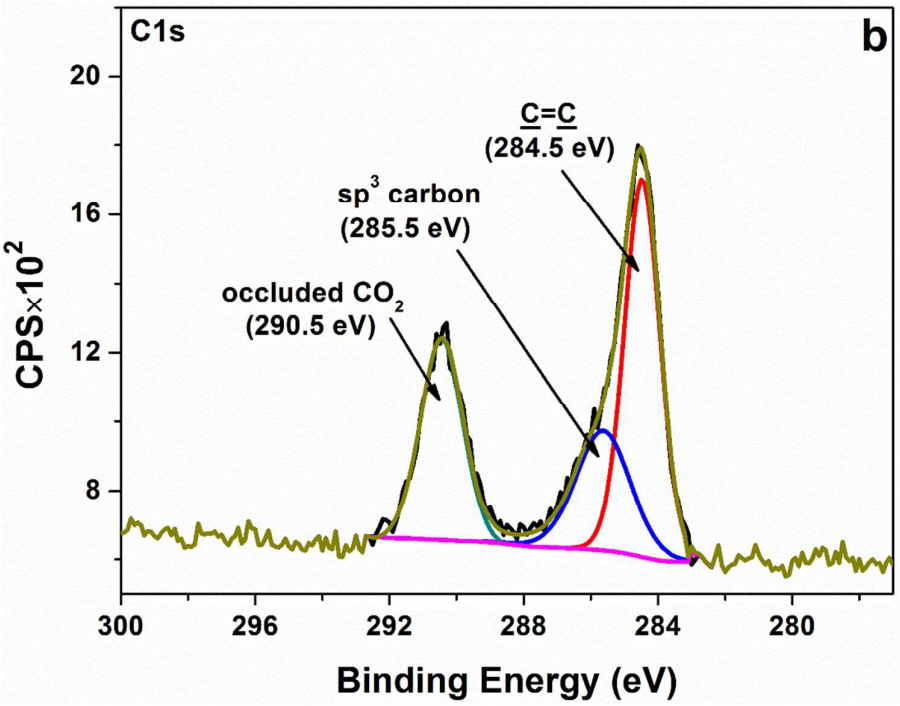

Fig. 4 XPS core level C1s spectrum of (a) Co-Ni and (b) Co-Ni-G.

Fig. 5a and 5b shows the core-level Co2p spectrum of Co-Ni alloy and Co-Ni-G composite coatings, respectively. It is possible to identify two species, metallic cobalt and cobalt oxide as evidenced by peaks at 778.2 eV and 781.1 eV, respectively.[39, 40] From Fig. 5a it can be seen that the ratio of peak area, $\left(\frac{A_{Co(0)}}{A_{Co(\text{II,III})}}\right)$ = 0.44 indicates an uneven distribution of Co(II, III) and Co(0) on the surface of Co-Ni electrode. From Fig. 5b it is observed that the ratio of peak area, $\left(\frac{A_{Co(0)}}{A_{Co(\text{II,III})}}\right)$ = 0.99, indicates an even distribution of Co(II, III) oxide and Co metal sites on the surface of Co-Ni-G electrode.

Fig. 5c and 5d shows the core-level Ni2p spectrum for deposits of Co-Ni alloy and Co-Ni-G composite coatings respectively. It is possible to identify two species, metallic nickel and nickel oxide as evidenced by peaks at 852.9 eV and 856.0 eV, respectively.[39, 41] From Fig. 5c it can be seen that the ratio of peak area, $\left(\frac{A_{Ni(0)}}{A_{Ni(\text{II})}}\right)$ = 0.31 indicates an uneven distribution of NiO and Ni metal on the surface of Co-Ni electrode. From Fig. 5d it is observed that the ratio of peak intensity $\left(\frac{A_{Ni(0)}}{A_{Ni(\text{II})}}\right)$ = 0.97, indicates an even distribution of NiO and Ni metal sites on the surface of Co-Ni-G electrode.

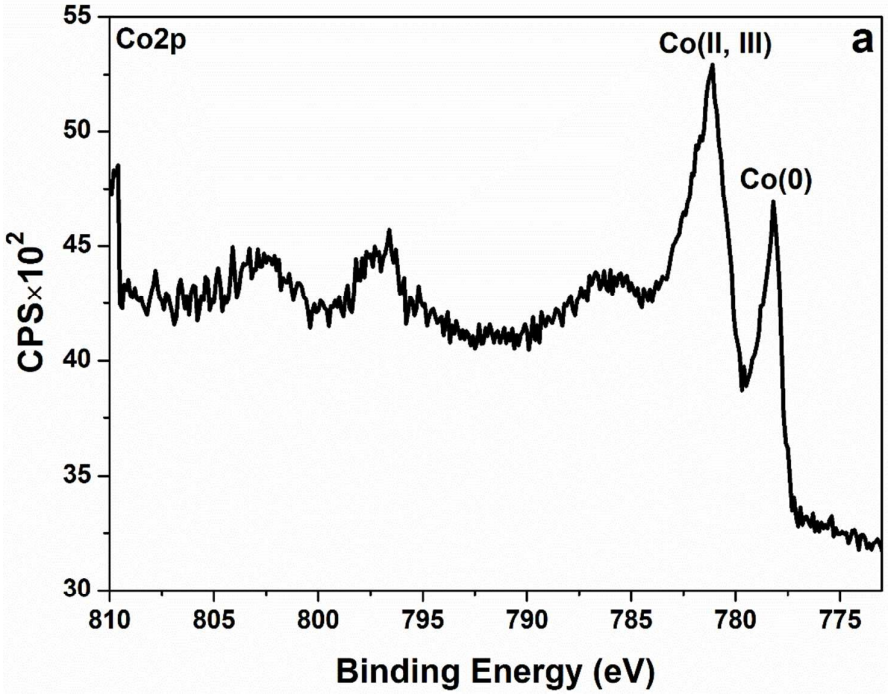

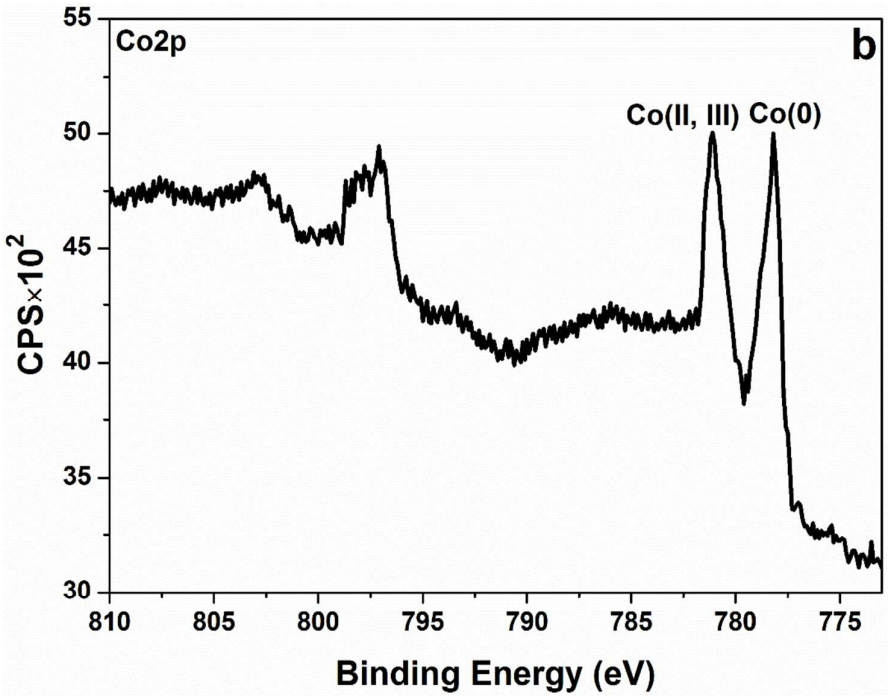

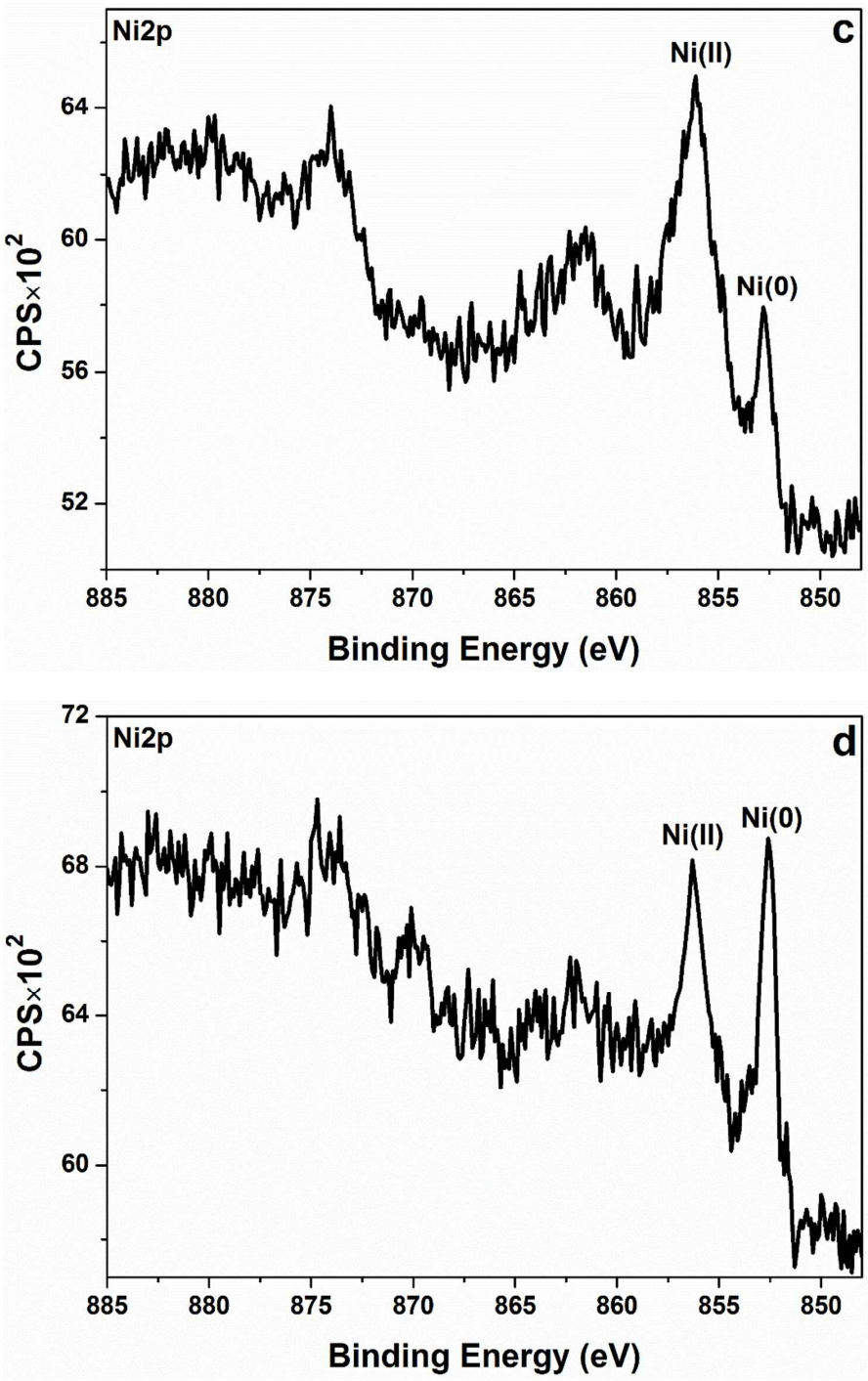

Fig. 5 XPS core level Co2p spectrum of (a) Co-Ni and (b) Co-Ni-G; XPS core level Ni2p spectrum of (c) Co-Ni and (d) Co-Ni-G.

XRD studies

The phase structure and grain size of the alloy and composite coatings were analyzed using XRD technique. The patterns for alloy and composite coatings are plotted to facilitate comparison (Fig. 6). The crystal structure of Co–Ni–G composite coating is mainly dependent on the cobalt content in the deposit. Since the composite coatings contain low wt.% of Co, it is confirmed the structure is single-phase solid solution of cobalt in nickel with a face-centered cubic (fcc) lattice that can be ascribed to the dominant influence of Ni atoms. The composite coating shows the presence of three well defined peaks of the fcc Ni structure at 44.7°, 51.8° and 76.4°, for the planes (111), (200) and (220) (JCPDS 04-0850), respectively, whereas for Co-Ni alloy coatings with high Co content a solid solution of nickel in cobalt with a hexagonal close packed (hcp) lattice

is obtained (JCPDS 01-089-7094).[42-46] The composite coatings at low current density values contain Ni (111) phase as preferred orientation and with the increase in deposition current density, the preferential orientation is more towards Ni (220) phase. All of the XRD patterns clearly show the diffraction peaks of the (111), (200) and (220) crystal planes at 37.24°, 43.3° and 62.88° respectively, corresponding to the fcc structure of the NiO (JCPDS 00-047-1049).[47] The peaks at 31.2°, 38.6° and 51.8° are assigned to diffraction from the (002) and (102) planes of hcp Co_2O_3 (JCPDS 00-002-0770), respectively.[48]

It is observed that, at both current densities, position of XRD signals remains almost unchanged with the addition of graphene, except for a broad peak at 2θ value of 24.5° corresponding to graphene.[49] It implies that the phase structure of Co-Ni alloy is not changed by the addition of graphene but it obviously influences the growth and orientation of crystal planes in composite coatings. Moreover, the peaks of composite coatings appeared to be slightly broadened than that of Co-Ni alloy coatings. This is attributed to the decrease in grain size of Co-Ni in the presence of graphene which is evident from the average grain sizes of the coatings calculated from the diffraction peak width using Scherrer equation (Eq. 4),

$$D_P = \frac{0.94\lambda}{\beta_{1/2}\cos\theta} \quad (4)$$

where D_p is crystallite size, λ is the wavelength of X-ray radaition, $\beta_{1/2}$ is the full width at half height of symmetrical shape of the diffraction peak and ϑ is the Bragg angle. The Co-Ni matrix in the composite coating had an average grain size of 38 nm, much smaller than that of the Co-Ni alloy coating (50 nm), electrodeposited under same conditions.

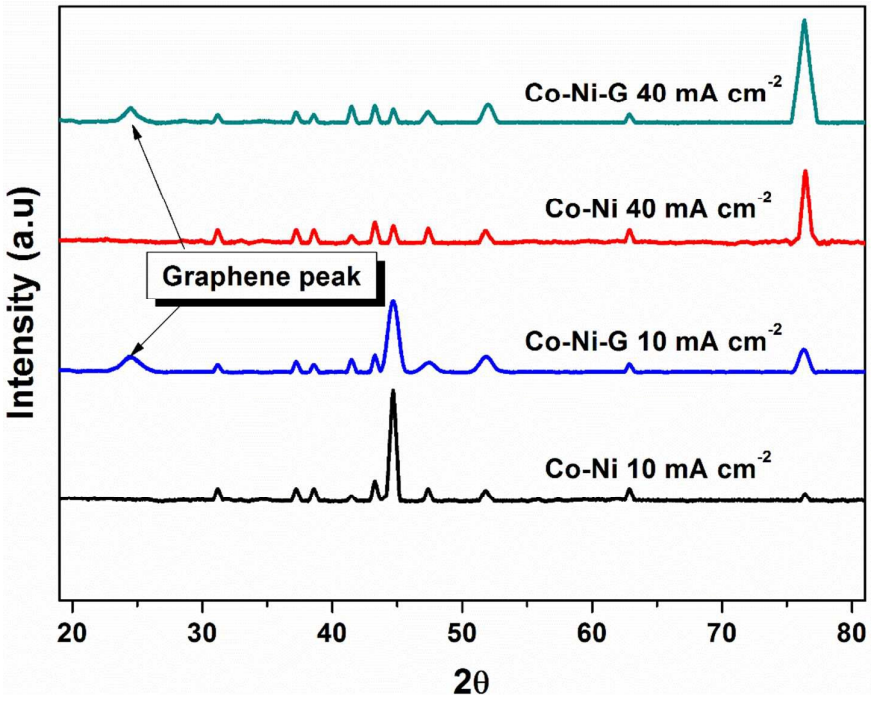

Fig. 6 XRD patterns of Co-Ni alloy and Co-Ni-G composite coatings deposited at different current densities.

Electrochemical characterization

Corrosion study

The corrosion resistance of Co-Ni coatings were evaluated in 6 M KOH electrolyte and is reported elsewhere by our group.[21] According to the reported data electrodeposited Co-Ni alloy coatings under working condition of its electro-catalytic behavior show least corrosion rate in the range of ~2.6 x 10^{-2} mm y^{-1}, well within the tolerable limit for electrode reactions. Hence the corrosion test of electrodeposited Co-Ni coatings qualifies them to be used as safe electrode material for water electrolysis in 6 M KOH.

Hydrogen evolution reaction

The HER of electrolytically coated Co-Ni-G composite coatings were studied in 6 M KOH electrolyte on 1.0 cm^2 effective geometric surface area. The experiments were performed by cyclic voltammetry and chrono-potentiometry methods and the results are discussed in the following sections.

Cyclic voltammetry study

The electrocatalytic HER in alkaline medium on Co-Ni-G composite coatings were studied by cyclic voltammetry (CV) in a three electrode cell. The experiment was carried out in 6 M KOH electrolyte between -0.5 V to -1.6 V vs. SCE at a scan rate of 50 mV s^{-1} for 50 cycles. It was observed in our previous study on Co-Ni alloy that towards the end of 50th cycle stable and reproducible CV curves were obtained with a state of equilibrium between formation/detachment of hydrogen bubbles (ESI†).[21] Hence CV curves of Co-Ni-G composite coatings deposited at different current densities, showing peak cathodic current densities (i_{pc}) for HER at the end of 50th cycle are shown in Fig. 7 and corresponding data are given in Table 2. It may be observed that at -1.6 V, i_{pc} for HER increases as the deposition current density increases and is approximately 4 times better than that of binary Co-Ni alloy coating (ESI†), as seen in Fig. 8. It may be attributed to the increased electrochemically active surface area of the electrode. It is supported by the increased area covered under the CV plot, as shown in Fig. 8.

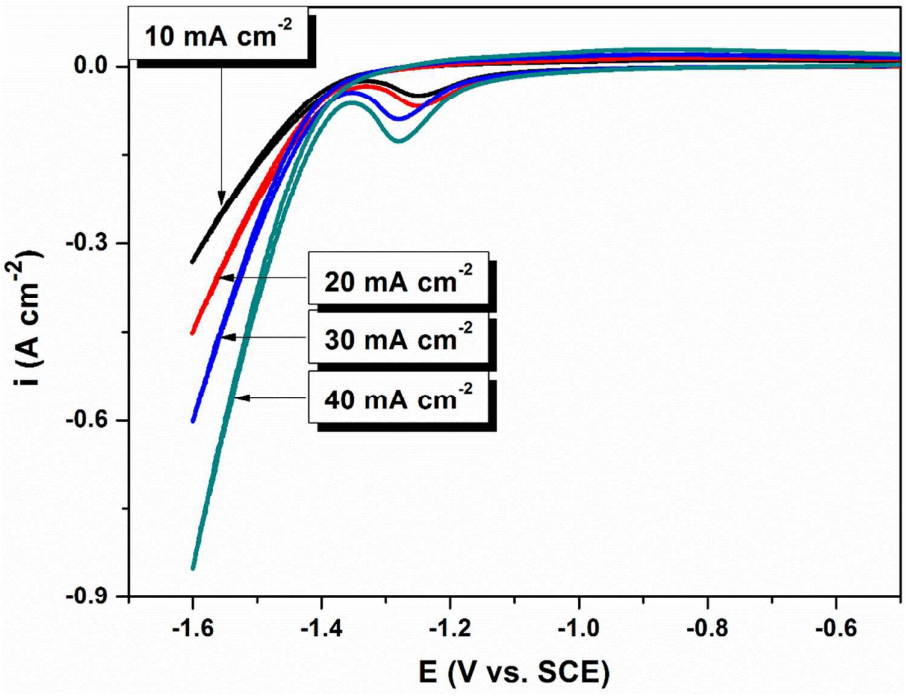

Fig. 7 CV curves depicting increase of i_{pc} with increase in deposition current density for Co-Ni-G composite coatings (on saturation after 50th cycle of CV).

Table 2 HER parameters for Co-Ni-G composite coatings developed at different current densities from optimal bath.

i (mA cm^{-2})	i_{pc} at -1.6 V (A cm^{-2})	Onset potential of H_2 evolution (V vs. SCE)	Volume of H_2 evolved in 300 s (cm^3)
10	-0.33	-1.21	10.1
20	-0.45	-1.18	12.3
30	-0.60	-1.17	15.0
40	-0.85	-1.15	20.1

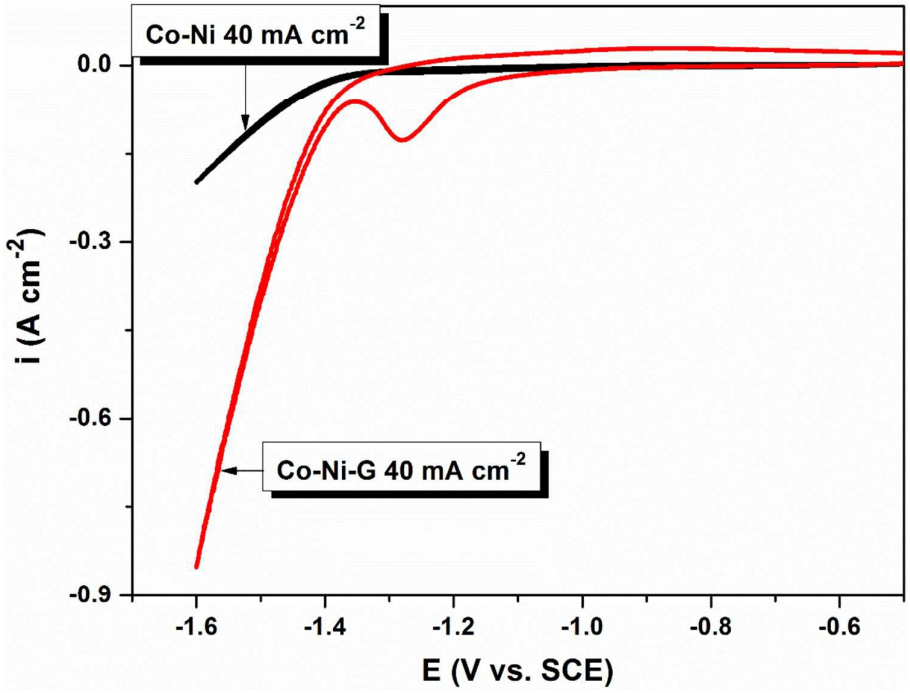

Fig. 8 Comparison of CV curves for HER on the surface of Co-Ni alloy and Co-Ni-G composite coatings (in 6 M KOH) deposited at same current density (40 mA cm^{-2}).

The FESEM image of Co-Ni-G coating (Fig. 2) shows encapsulated bundle of alloy nano-particles within the graphene network. Thus the surface roughness of the coating is greatly enhanced by the addition of graphene. This results in increase of electrochemically active surface area and in turn increases the electrocatalytic activity of the composite electrode. Also XPS analysis reveals that the addition of graphene increases the Co(0) and Ni(0) content in the deposit. The increase in metallic nickel and cobalt content accelerates the rate determining proton discharge reaction (Volmer reaction) as a result of enhanced charge transfer thereby contributing for increased HER activity of the Co-Ni-G composite electrode.[50]

In alkaline media, the HER pathway could be through the Volmer–Tafel (Eq. 1 & 3) process or Volmer–Heyrovsky (Eq. 1 & 2) pathways. Both pathways involve the adsorption of H_2O molecule, electrochemical reduction of adsorbed H_2O into adsorbed OH^- and H atom, desorption of OH^- to refresh the surface and formation of H adsorbed intermediate for H_2 generation. A pure metal oxide surface is not active for HER due to the lack of H adsorption sites. On a pure metal surface without any metal oxide, the adsorbed OH^- species could occupy the sites for H atom, causing inefficient release of OH^- and blocking of the active catalytic sites. Therefore, for an effective increase in HER catalytic activity, even distribution of metal oxide and pure metal is necessary.[51] As indicated by XPS analysis results, both cobalt/cobalt oxide and nickel/nickel oxide sites are evenly distributed on the surface of Co-Ni-G electrode which is responsible for the increased HER activity of the composite electrode.

The kinetic behavior of the electrocatalysts developed under different deposition conditions were evaluated by analyzing the Tafel slope and is shown in Fig. 9. The exchange current densities were calculated by Butler-Volmer equation and the values were in good agreement with values obtained from CV study. In each plot corresponding to different coatings, it may be seen that the first step is an electro-reduction of the water molecule, with the formation of hydrogen adsorbed on the electrode surface (Volmer reaction), followed by an electrochemical (Heyrovsky reaction), and/or chemical (Tafel reaction) desorption of H_2. Analysis of the HER mechanism for Co-Ni and Co-Ni-G coatings have been made based on Tafel slope (β_c) values.[52] Tafel slope (β_c) and exchange current density (i_o) corresponding to Co-Ni alloy and Co-Ni-G composite coatings were determined from Tafel plot (Fig. 9) and the values are reported in Table 3. It may be noted that all the slope values are in the range of -118 mV per decade confirming that the HER on these coatings follows Volmer-Tafel mechanism.[53] The increase of exchange current density for coatings containing graphene indicates that they are more efficient in producing hydrogen on their surface.

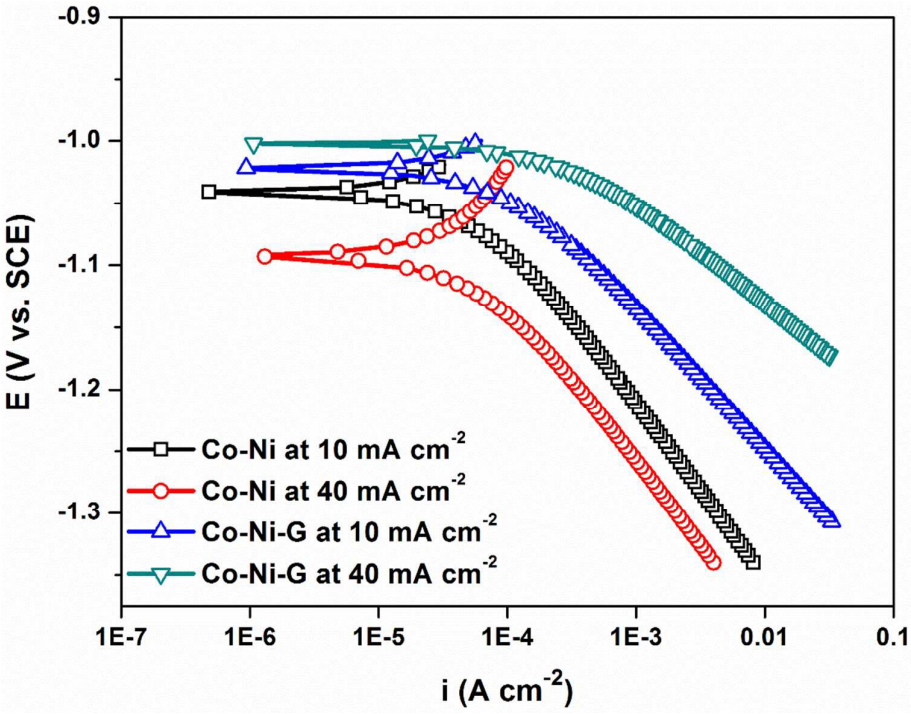

Fig. 9 Comparison of Tafel slopes (β_c) for HER on electroactive coatings of Co-Ni and Co-Ni-G developed under different current densities.

Table 3 Tafel slope (β_c) and exchange current density (i_o) of Co-Ni alloy and Co-Ni-G composite coatings developed under different current densities.

Electrodeposit coating configuration	Tafel slope, β_c (mV dec^{-1})	i_o (μA cm^{-2})
$(Co\text{-}Ni)_{10\ mA\ cm^{-2}}$	-115.6	60.4
$(Co\text{-}Ni)_{40\ mA\ cm^{-2}}$	-97.2	200.3
$(Co\text{-}Ni\text{-}G)_{10\ mA\ cm^{-2}}$	-105.3	68.4
$(Co\text{-}Ni\text{-}G)_{40\ mA\ cm^{-2}}$	-84.5	235.4

Chrono-potentiometry

Usually, conventional low-pressure alkaline electrolysers for industrial purpose operate at current densities from -100 mA cm^{-2} to -300 mA cm^{-2}. The simplest way to estimate the electrocatalytic activity under these conditions is to monitor the electrode potential at constant current density applied over sufficient period of time by chrono-potentiometry experiment.[52] The chrono-potentiometry study for the evolution of hydrogen on Co-Ni-G composite coatings, deposited at different current densities, were made at a constant current of 300 mA cm^{-2} for a duration of 1500 s. The electrocatalytic behavior of each of the coatings was evaluated by measuring the amount of H_2 liberated in first 300 s. The nature of chrono-potentiograms for Co-Ni alloy and Co-Ni-G composite coatings deposited at 40 mA cm^{-2} are shown in Fig. 10. The electrodeposited catalysts show low potential for HER in the initial period and then the potential slowly stabilized. This phenomenon is ascribed to the formation of hydrogen bubble on the surface of the electrode. The inset chart in Fig. 10 shows the volume of H_2 liberated in 300 s on each coating deposited at different current densities with and without graphene. It is observed that on increasing the current density the volume of H_2 evolved increases; but not linearly proportionate to the increase in current density. This can be explained as follows: As electrolysis progresses, hydrogen gas bubbles are formed on the surfaces of the cathode and are only detached from the surface when they grow big enough. The coverage of the electrode surfaces by the gas bubbles directly adds to the electrical resistance of the whole system, by reducing the contact between the electrolyte and the electrode, blocking the electron transfer and increasing the ohmic

loss of the whole system and results in higher energy consumption.[54] It may be seen that the coating corresponding to 40 mA cm^{-2} shows maximum H_2 evolution, due to excess porosity of the coating. Further, Co-Ni-G composite coatings showed substantial reduction in the hydrogen evolution potential of 140 mV (Table 2) as compared to its binary alloy (Co-Ni) electrocatalyst (ESI†).[21] Also, the volume of hydrogen gas liberated in 300 s is found to be much higher in the case of composite coatings, as shown graphically in inset of Fig. 10.

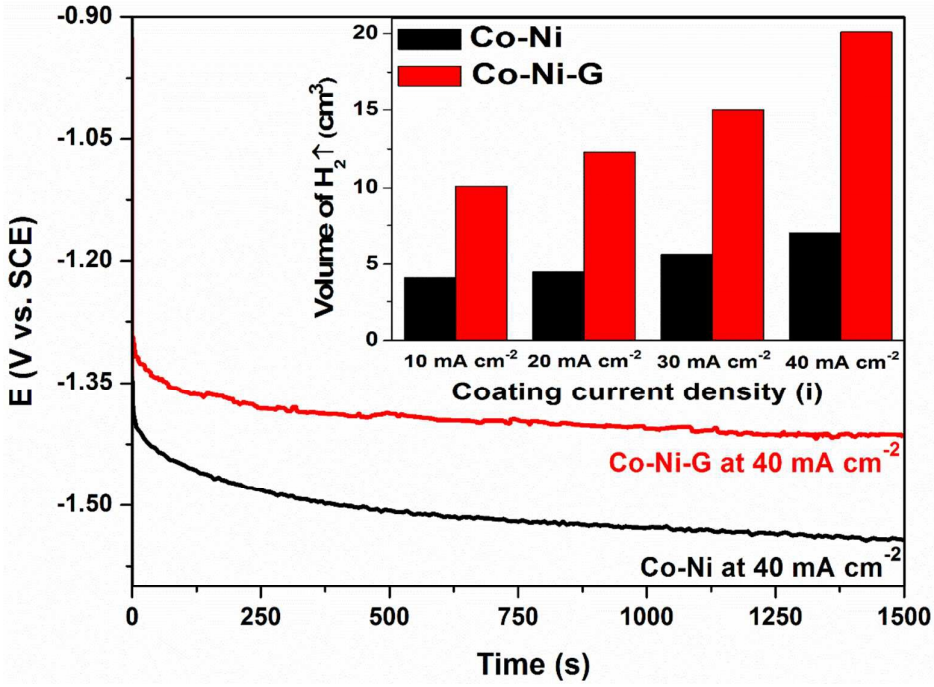

Fig. 10 Chrono-potentiometry curves at -300 mA cm^{-2} recorded using Co-Ni alloy and Co-Ni-G composite coatings developed at 40 mA cm^{-2}. The inset chart shows the volume of H_2 liberated in 300 s on each of the coatings deposited at different current densities.

Comparison of Co-Ni-G system with Platinum based materials for HER

Pt-based materials are characterized by lowest overpotential and highest exchange current density for water electrolysis in alkaline medium.[6, 55-58] Hence they are the most efficient catalysts for electrochemical water splitting. But low abundance, high cost and surface poisoning (e.g. by CO) suggest that these catalysts cannot be used on a large scale.[59-62] Although Co-Ni-G composite electrode has higher overpotential (approx. -1.2 V) and lower exchange current density as compared to Pt-based materials, it does not get easily deactivated by adsorption of poisonous intermediates or reaction products (e.g. CO), thus increasing the active sites for reactant molecules. Unlike Platinum, Co-Ni-G catalyst combines the ability to oxidize both CO and H_2O effectively.[59] Moreover it is made up of earth-abundant elements and hence is way more economical than Pt-based materials. Also unlike the catalytic reaction on Pt, increasing the concentration of water molecules at the surface favours water-splitting on graphene-based catalysts.[63]

The disadvantages of Co-Ni-G system when compared to Pt-based materials are listed below:

- Co-Ni-G electrode has high overpotential for HER reaction when compared with Pt-based materials.
- They are not stable in acids and therefore incompatible with proton exchange membrane based electrolysis units, which are very compact and have the potential to lower the overall capital cost.[64]
- The durability is still not satisfactory in strongly acidic electrolytes under the long-time operation or accelerated degradation measurements.[65]
- Also, deactivation is caused by the high hydrogen concentration near the electrode, which leads to the formation of a Ni hydride phase at the surface.[66]

Conclusions

In conclusion, we have demonstrated a simple electrochemical method to synthesize a novel electrocatalyst consisting of graphene layers (1-2 layers) that encapsulate a uniform Co-Ni nanoalloy. The results indicate that the incorporation of graphene into Co-Ni alloy matrix enhances the catalyst activity in HER performance of the composite electrode. The best

coating exhibits a maximum current density of -850 mA cm^{-2} at -1.6 V, which is approximately 4 times better than that of binary Co-Ni alloy indicating higher activity for hydrogen production. As indicated by XPS analysis results, on addition of graphene, Co(0) and Ni(0) content in the deposit increases and as a result both cobalt/cobalt oxide and nickel/nickel oxide sites are evenly distributed on the surface of Co-Ni-G composite electrode. Also the deposition of metallic cobalt/nickel is favored on the addition of graphene which accelerates the rate determining proton discharge reaction. All these factors remarkably enhance the HER activity of Co-Ni-G composite electrode. Under the studied range of current density Co-Ni-G composite coating developed at 40 mA cm^{-2} was found to be efficient electrode material for HER reaction as demonstrated by cyclic voltammetry and chrono-potentiometry experiments. The Tafel slope analysis shows that the HER follows Volmer-Tafel mechanism.

Acknowledgments

The authors would like to thank Indian Institute of Technology-Bombay and Centre for Nanoscience and Engineering-IISc, Bangalore for providing necessary characterization facilities. BS and YU are grateful to National Institute of Technology Karnataka-Surathkal, for providing financial assistance in the form of Institute fellowship along with necessary facilities and infrastructure to carry out the present work. Special thanks to Dr. David J Morgan, Postdoctoral Research Associate, Cardiff Catalysis Institute, School of Chemistry, Cardiff University and Mr. Rajkamal Balu, PhD Student, Ian Wark Research Institute, University of South Australia for extending help in the interpretation of XPS results.

Notes and references

†Electronic Supplementary Information (ESI) available: Synthesis of Graphene, surface and compositional characterization of Co-Ni alloy coatings, electrochemical characterization of Co-Ni alloy coatings.

1. N. S. Lewis and D. G. Nocera, *Proc. Natl. Acad. Sci.*, 2006, **103**, 15729-15735.
2. M. S. Dresselhaus and I. L. Thomas, *Nature*, 2001, **414**, 332-337.
3. J. A. Turner, *Science*, 1999, **285**, 687-689.
4. J. A. Turner, *Science*, 2004, **305**, 972-974.
5. Y. Zheng, Y. Jiao, M. Jaroniec and S. Z. Qiao, *Angew. Chem. Int. Ed.*, 2015, **54**, 52-65.
6. W. Sheng, H. A. Gasteiger and Y. Shao-Horn, *J. Electrochem. Soc.*, 2010, **157**, B1529-B1536.
7. B. E. Conway and B. V. Tilak, *Electrochim. Acta*, 2002, **47**, 3571-3594.
8. Y. Sun, M. Delucchi and J. Ogden, *Int. J. Hydrogen Energy*, 2011, **36**, 11116-11127.
9. P. Du and R. Eisenberg, *Energy Environ. Sci.*, 2012, **5**, 6012-6021.
10. R. Subbaraman, D. Tripkovic, K.-C. Chang, D. Strmcnik, A. P. Paulikas, P. Hirunsit, M. Chan, J. Greeley, V. Stamenkovic and N. M. Markovic, *Nat. Mater.*, 2012, **11**, 550-557.
11. J. R. McKone, S. C. Marinescu, B. S. Brunschwig, J. R. Winkler and H. B. Gray, *Chem. Sci.*, 2014, **5**, 865-878.
12. S. H. Ahn, S. J. Hwang, S. J. Yoo, I. Choi, H.-J. Kim, J. H. Jang, S. W. Nam, T.-H. Lim, T. Lim, S.-K. Kim and J. J. Kim, *J. Mater. Chem.*, 2012, **22**, 15153-15159.
13. O. Savadogo and H. Lavoie, *Int. J. Hydrogen Energy*, 1992, **17**, 473-477.
14. O. Savadogo and F. Carrier, *J. Appl. Electrochem.*, 1992, **22**, 437-442.
15. C. Fan, D. L. Piron, A. Sleb and P. Paradis, *J. Electrochem. Soc.*, 1994, **141**, 382-387.
16. J. Kubisztal, A. Budniok and A. Lasia, *Int. J. Hydrogen Energy*, 2007, **32**, 1211-1218.
17. K. Ngamlerdpokin and N. Tantavichet, *Int. J. Hydrogen Energy*, 2014, **39**, 2505-2515.
18. C. Fan, D. L. Piron and P. Paradis, *Electrochim. Acta*, 1994, **39**, 2715-2722.
19. N. V. Krstajić, V. D. Jović, L. Gajić-Krstajić, B. M. Jović, A. L. Antozzi and G. N. Martelli, *Int. J. Hydrogen Energy*, 2008, **33**, 3676-3687.
20. S. J. Hwang, S. J. Yoo, S. Jang, T.-H. Lim, S. A. Hong and S.-K. Kim, *J. Phys. Chem. C*, 2011, **115**, 2483-2488.
21. Y. Ullal and A. C. Hegde, *J. Electrochem. Plat. Technol*., 2014, **25**, 1-14.
22. Y. Zheng, Y. Jiao, L. H. Li, T. Xing, Y. Chen, M. Jaroniec and S. Z. Qiao, *ACS Nano*, 2014, **8**, 5290-5296.
23. Y. Zheng, Y. Jiao, Y. Zhu, L. H. Li, Y. Han, Y. Chen, A. Du, M. Jaroniec and S. Z. Qiao, *Nat. Commun.*, 2014, **5**, 3783.
24. A. K. Geim and K. S. Novoselov, *Nat. Mater.*, 2007, **6**, 183-191.
25. K. S. Novoselov, A. K. Geim, S. V. Morozov, D. Jiang, Y. Zhang, S. V. Dubonos, I. V. Grigorieva and A. A. Firsov, *Science*, 2004, **306**, 666-669.
26. M. D. Stoller, S. Park, Y. Zhu, J. An and R. S. Ruoff, *Nano Lett.*, 2008, **8**, 3498-3502.
27. J. H. Chen, M. Ishigami, C. Jang, D. R. Hines, M. S. Fuhrer and E. D. Williams, *Adv. Mater.*, 2007, **19**, 3623-3627.
28. F. Schedin, A. K. Geim, S. V. Morozov, E. W. Hill, P. Blake, M. I. Katsnelson and K. S. Novoselov, *Nat. Mater.*, 2007, **6**, 652-655.
29. G. Eda and M. Chhowalla, *Nano Lett.*, 2009, **9**, 814-818.
30. Q. Li, B. Guo, J. Yu, J. Ran, B. Zhang, H. Yan and J. R. Gong, *J. Am. Chem. Soc*., 2011, **133**, 10878-10884.
31. B. Subramanya and D. K. Bhat, *J. Power Sources*, 2015, **275**, 90-98.
32. B. Subramanya and D. K. Bhat, *New J. Chem.*, 2015, **39**, 420-430.

33. H. B. Suffredini, J. L. Cerne, F. C. Crnkovic, S. A. S. Machado and L. A. Avaca, *Int. J. Hydrogen Energy*, 2000, **25**, 415-423.
34. F. C. Crnkovic, S. A. S. Machado and L. A. Avaca, *Int. J. Hydrogen Energy*, 2004, **29**, 249-254.
35. N. Kanani, in *Electroplating*, ed. N. Kanani, Elsevier, Oxford, 2004, DOI: http://dx.doi.org/10.1016/B978-185617451-0/50003-8, pp. 55-85.
36. C. K. Chua and M. Pumera, *J. Mater. Chem.*, 2012, **22**, 23227-23231.
37. C. Hontoria-Lucas, A. J. López-Peinado, J. d. D. López-González, M. L. Rojas-Cervantes and R. M. Martín-Aranda, *Carbon*, 1995, **33**, 1585-1592.
38. M.-C. Hsiao, S.-H. Liao, M.-Y. Yen, C.-C. Teng, S.-H. Lee, N.-W. Pu, C.-A. Wang, Y. Sung, M.-D. Ger, C.-C. M. Ma and M.-H. Hsiao, *J. Mater. Chem.*, 2010, **20**, 8496-8505.
39. M. C. Biesinger, B. P. Payne, A. P. Grosvenor, L. W. M. Lau, A. R. Gerson and R. S. C. Smart, *Appl. Surf. Sci.*, 2011, **257**, 2717-2730.
40. J. Yang, H. Liu, W. N. Martens and R. L. Frost, *J. Phys. Chem. C*, 2009, **114**, 111-119.
41. L. S. Sanches, C. E. Marino and L. H. Mascaro, *Int. J. Electrochem. Sci*, 2012, **7**, 9213-9220.
42. G. Wu, N. Li, D. Zhou and K. Mitsuo, *Surf. Coat. Technol.*, 2004, **176**, 157-164.
43. M. Spasojevic, L. Ribic-Zelenovic and A. Maricic, *Sci. Sinter.*, 2011, **43**, 313-327.
44. J. García, V. Vega, L. Iglesias, V. M. Prida, B. Hernando, E. D. Barriga-Castro, R. Mendoza-Reséndez, C. Luna, D. Görlitz and K. Nielsch, *Phys. Status Solidi A*, 2014, **211**, 1041-1047.
45. G. Qiao, T. Jing, N. Wang, Y. Gao, X. Zhao, J. Zhou and W. Wang, *Electrochim. Acta*, 2005, **51**, 85-92.
46. M. Srivastava, V. Ezhil Selvi, V. K. William Grips and K. S. Rajam, *Surf. Coat. Technol.*, 2006, **201**, 3051-3060.
47. W.-X. Chen, G.-L. Zhuang, H.-X. Zhao, L.-S. Long, R.-B. Huang and L.-S. Zheng, *Dalton Trans.*, 2011, **40**, 10237-10241.
48. M. Zabihi, F. Khorasheh and J. Shayegan, *RSC Advances*, 2015, **5**, 5107-5122.
49. A. Kaniyoor, T. T. Baby and S. Ramaprabhu, *J. Mater. Chem.*, 2010, **20**, 8467-8469.
50. S. Meguro, T. Sasaki, H. Katagiri, H. Habazaki, A. Kawashima, T. Sakaki, K. Asami and K. Hashimoto, *J. Electrochem. Soc.*, 2000, **147**, 3003-3009.
51. M. Gong, W. Zhou, M.-C. Tsai, J. Zhou, M. Guan, M.-C. Lin, B. Zhang, Y. Hu, D.-Y. Wang, J. Yang, S. J. Pennycook, B.-J. Hwang and H. Dai, *Nat. Commun.*, 2014, **5**, 4695.
52. G. S. Tasić, U. Lačnjevac, M. M. Tasić, M. M. Kaninski, V. M. Nikolić, D. L. Žugić and V. D. Jović, *Int. J. Hydrogen Energy*, 2013, **38**, 4291-4297.
53. Y. Choquette, L. Brossard, A. Lasia and H. Menard, *J. Electrochem. Soc.*, 1990, **137**, 1723-1730.
54. K. Zeng and D. Zhang, *Prog. Energy Combust. Sci.*, 2010, **36**, 307-326.
55. A. Lasia, in *Handbook of Fuel Cells*, John Wiley & Sons, Ltd, 2010, DOI: 10.1002/9780470974001.f204033.
56. J. Durst, A. Siebel, C. Simon, F. Hasche, J. Herranz and H. A. Gasteiger, *Energy Environ. Sci.*, 2014, **7**, 2255-2260.
57. N. M. Markovica, S. T. Sarraf, H. A. Gasteiger and P. N. Ross, *J. Chem. Soc., Faraday Trans.*, 1996, **92**, 3719-3725.
58. M. Metikoš-Huković, Z. Grubač, N. Radić and A. Tonejc, *J. Mol. Catal. A: Chem.*, 2006, **249**, 172-180.
59. H. Wolfschmidt, O. Paschos and U. Stimming, in *Fuel Cell Science*, John Wiley & Sons, Inc., 2010, DOI: 10.1002/9780470630693.ch1, pp. 1-70.
60. Q. Li, R. He, J.-A. Gao, J. O. Jensen and N. J. Bjerrum, *J. Electrochem. Soc.*, 2003, **150**, A1599-A1605.
61. J. Grunes, J. Zhu, M. Yang and G. Somorjai, *Catal. Lett.*, 2003, **86**, 157-161.
62. D. S. Su, S. Perathoner and G. Centi, *Chem. Rev.*, 2013, **113**, 5782-5816.
63. D. W. Boukhvalov, Y. W. Son and R. S. Ruoff, *ACS Catalysis*, 2014, **4**, 2016-2021.
64. D. Kong, J. J. Cha, H. Wang, H. R. Lee and Y. Cui, *Energy Environ. Sci.*, 2013, **6**, 3553-3558.
65. J. Deng, P. Ren, D. Deng, L. Yu, F. Yang and X. Bao, *Energy Environ. Sci.*, 2014, **7**, 1919-1923.
66. R. M. Abouatallah, D. W. Kirk and J. W. Graydon, *Electrochim. Acta*, 2002, **47**, 2483-2494.